# Solar module defects classification using deep convolutional neural network



Rizqia Cahyaningtyas a,1,\*, Sarifuddin Madenda a,2, Bertalya a,3, Dina Indarti a,4

- <sup>a</sup> Gunadarma University, Jl. Margonda Raya 100, Depok 16424, Indonesia
- <sup>1</sup> r<mark>izqia@itpln.ac.id; ² sarif@staff.gunadarma.ac.id; ³ bertalya@staff.gunadarma.ac.id; ⁴ dina\_indarti@staff.gunadarma.ac.id</mark>
- \* corresponding author

#### ARTICLE INFO

#### **Article history**

Received October 27, 2024 Revised July 11, 2025 Accepted July 25, 2025 Available online August 31, 2025

#### Keywords

Classification Deep convolutional neural network Solar module Transfer learning The defect types

#### ABSTRACT

Solar modules are essential components of a solar power plant, that are designed to withstand scorching heat, storms, strong winds, and other natural influences. However, continuous usage can cause defects in solar modules, preventing them from producing electrical energy optimally. This paper proposes the development of a deep learning-based system for identifying and classifying solar module surface defects in solar power plants. Module surface condition are classified into five categories: clean, dirt, burn, crack, and snail track. The dataset used consists of 8,370 images, including primary image data acquired directly from the mini solar power plant at the Renewable Energy Laboratory of PLN Institute of Technology, and secondary image data obtained from public repositories. The limitation in the number of images in each category was overcome using data augmentation techniques. The proposed classification model combines Deep Convolutional Neural Networks (DCNN) with transfer learning models (DenseNet201, MobileNetV2, and EfficientNetB0) to perform supervised image classification. Training and testing results on the three models demonstrated that the combination of DCNN + DenseNet201 provided the best performance, with a classification accuracy of 97.85%, compared to 97.25% accuracy for DCNN + EfficientNetB0 and 94.98% for DCNN + MobileNetV2. This research shows that DCNN-based image classification reliably diagnoses solar module defects and supports using RGB images for surface defect classification. Applying the developed system to solar power plant maintenance management can help in accelerating the process of identifying panel defects, determining defect types, and performing panel maintenance or repairs, while ensuring optimal power production.



© 2025 The Author(s). This is an open access article under the CC-BY-SA license.



#### 1. Introduction

The Solar Power Plant has been the subject of several studies in the world of ICT [1], [2]. The solar module is a critical component of Solar Power Plant systems [3]-[5], designed to directly convert solar radiation into electrical energy, to meet human needs [6], [7]. These modules are engineered to endure extreme environmental conditions such as intense heat, rainstorms, and strong winds. Their operational lifespan is estimated to reach 25 years, with an annual power loss of approximately 0.8% [8], [9]. However, without proper maintenance, they remain prone to various types of surface damage [10].

Common surface defects include broken or crack [11], [12], hotspots [13], [14], burn [15], snail tracks [16], microcracks [17], [18], and accumulated dust or dirt [19], [20]. Certain issues, such as delamination or deglazing, may begin as minor faults but eventually evolve into more severe defects, thus







reducing the efficiency and lifespan of the module [21]. To prevent such degradation, continuous performance monitoring and predictive maintenance are essential [22], [23].

Currently, visual inspections are predominantly manual and reliant on human observation, which is inherently subjective, time-consuming, and error-prone. As an alternative, deep learning has shown significant potential in managing visual challenges, including tasks of classification, detection, and forecasting in real-life applications [24]–[26]. Convolutional Neural Networks (CNNs) are among the most effective deep learning architectures for processing visual data [27]–[29]. They can analyze images to uncover underlying structures and visual elements [30], [31]. making them suitable for monitoring and detecting damage or interference in solar modules [32].

To enhance classification efficiency and reduce training time, transfer learning is often used to adapt pretrained models (commonly Imagenet) to solve challenges on other datasets [33], [34]. CNN architectures such as DenseNet121 [35], [36], MobileNetV2 [37], [38], and EfficientNetB0 [39], [40]They have achieved high accuracy in various image classification domains and are promising for adaptation to solar module defect detection.

Several prior studies have examined CNN-based defect detection in photovoltaic modules [41]. One research explicitly focused on crack detection using electroluminescence (EL) images [42]. Various defect types, such as microcracks and potential-induced degradation (PID), were investigated using six different CNN architectures applied to EL inputs [43]. Thermal imaging was utilized to identify faults during the manufacturing stage [44]. while multispectral CNNs were employed to detect surface defects [45]. Other studies developed CNN-based models to recognize specific surface anomalies, including dust and discoloration [46]. Enhancing generalization and addressing overfitting concerns, several data augmentation techniques were introduced during the training phase [47].

However, a clear gap remains in research utilizing real-world RGB imagery of solar modules captured under diverse field conditions. While most prior work relies on controlled laboratory environments using EL or thermal imagery, this research addresses the need for RGB-based classification under natural conditions, focusing on five common surface failures: clean, dirt, burn, crack, and snail track. The dataset combines field-acquired images and publicly available sources enhanced through structured data augmentation techniques to mitigate class imbalance and improve model generalization. This research aims to develop a CNN-based classification model using transfer learning on these RGB datasets and to evaluate model performance through hyperparameter tuning to identify the most effective architecture for accurate surface defect classification.

## 2. Method

The purpose of this work is to develop a deep learning approach using CNNs with transfer learning to automate the classification of solar module surface faults.

Fig. 1 illustrates the research stages conducted to achieve the research's objectives. The initial step involved acquiring RGB images corresponding to five types of surface conditions: clean, dirt, burn, crack, and snail track, from both primary and secondary sources. Primary data were collected directly from the mini solar power plant at the Renewable Energy Laboratory of PLN Institute of Technology, while secondary data were obtained from public repositories such as Kaggle [48] and Roboflow [49]. During the data preparation phase, the images were cleaned to remove noise and artifacts, augmented to address data imbalance, normalized to a pixel value range of [0,1], resized to 224×224 pixels, and then divided into training, validation, and testing subsets. Next, three pretrained CNN architectures (DenseNet201, MobileNetV2, and EfficientNetB0) were employed using a transfer learning approach. The final classification layers of these models were modified to accommodate the five target classes, and several hyperparameter tuning scenarios were applied to optimize their performance. The models were evaluated using accuracy, precision, recall, and F1-score, with the best-performing model selected as the final classifier for detecting surface defects in solar modules.

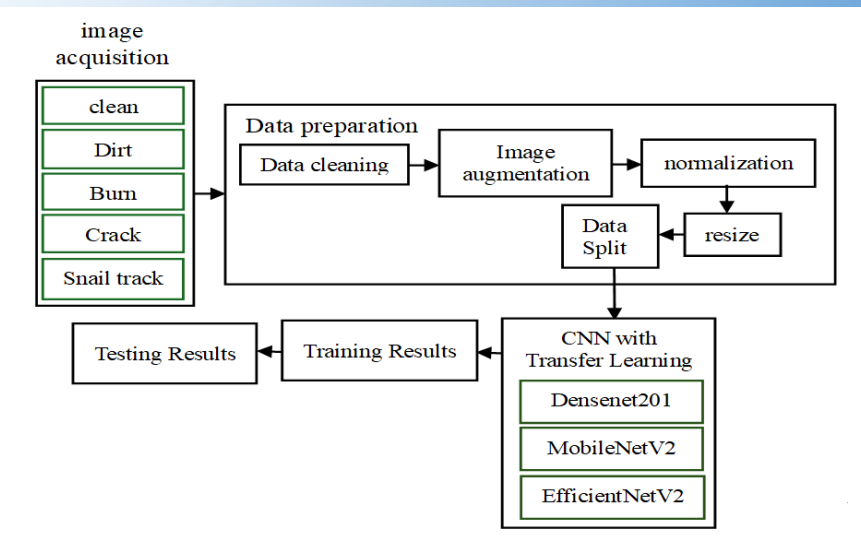


Fig. 1. The research stage

## 2.1. Image Acquisition

The data acquisition and analysis phase began with collecting surface condition of the solar module, from both primary and secondary. Primary data were obtained from the mini solar power plant at PLN Institute of Technology using both monocrystaline and polycrystaline solar modules Images of the solar module surface conditions were captured using a high-resolution camera, from various viewpoints, at different height, and under various natural lighting conditions such as direct sunlight, overcast skies, and mild partial shading. This approach aimed to increase the diversity and representativeness of the dataset. Secondary data were sourced from Kaggle and Roboflow in .jpg, .jpeg, and .png formats using the RGB color space [50]. The surface conditions of the solar modules were categorized into five classes: clean, dirt, burn, crack, and snail track. The initial dataset consisted of 3,800 images, comprising 1,290 primary images and 2,510 secondary images.

## 2.2. Data Preparation

Some primary and secondary data were cleaned of errors, inconsistencies, and anomalies which may influence the precision and consistency of the analytical outcomes. Image cleaning was applied to remove photos that displayed module arrays or circuits, as well as those affected by excessive shadows, strong reflections, or glare that obscured the true surface condition. Such lighting artifacts were treated as noise rather than meaningful variations, ensuring consistent and reliable visual input for surface defect classification. A total of 198 images were removed during the cleaning process, decreasing the dataset size from 3,800 to 3,602.

The number of each category indicates a data imbalance problem. The imbalance of data in this research was addressed by using augmentation techniques, which can also balance the amount of data, improve data quality, and feature representation [51]. In each augmentation iteration, an image underwent one to three randomly selected transformations to create various new image versions. After augmentation, the data were accumulated and saved, aiming to equalize the sample count across categories by matching the largest original class size.

To address class imbalance, augmentation techniques were applied, including Gaussian blur ( $\sigma \in [0, 1.0]$ ), random rotation (±20°), Gaussian noise (0 – 5% intensity), brightness adjustment (80 – 120% scale), and horizontal flipping (50% probability). Each category was balanced to 1,674 images postaugmentation.

The next step was data normalization [52], where pixel values were normalized by rescaling them from their original 0–255 range to the 0–1 interval [53]. Since each pixel in a color image has an intensity value across three channels (Red, Green, Blue), normalization was performed by dividing each value by 255. This step is essential for accelerating convergence during training [54].

The dataset's image size varies. Hence, it be equalized to 224×224 [55]. Image size equalization aims to ensure consistency of input images during the model training process, therefore speeding up the training process, reducing data complexity and computational load, and allowing models to focus on important features, increasing models' ability to generalize to new data.

The dataset was split into three parts: 80% for training, 10% for testing, and the rest allocated for validation. The validation set size was computed proportionally based on the remaining data after extracting the training set.

Two experiments were conducted. In the initial experiment, the original dataset comprising 3,602 images was utilized and systematically divided into 2,881 training samples, 360 testing samples, and 361 validation samples. In contrast, the second experiment employed an augmented dataset totaling 8,370 images, which was partitioned into 6,696 for training, 837 for testing, and 837 for validation. A detailed breakdown of the dataset allocation is provided in Table 1.

Table 1. Data Split

No	Description	Number of Datasets	Data Training	Data Validation	Data Testing
1	The original dataset	3602	2881	361	360
2	Datasets using augmentation	8370	6696	837	837

## 2.3. CNN with Transfer Learning

The next stage after the dataset preparation stage is the CNN model architecture. At this stage several experiments were carried out using three CNN models, namely DenseNet201, MobilenetV2, and EfficientNetB0 to obtain the optimal model in classifying solar module defects. The selection of DenseNet201, MobileNetV2, and EfficientNetB0 in this research was based on the distinct advantages offered by each architecture in image classification tasks. DenseNet201 was chosen for its deep network structure and efficient feature propagation through direct connections between layers, making it well-suited for capturing complex patterns in solar module surface images [56]. MobileNetV2 is a compact and efficient architecture, well-suited for implementation on devices with limited computational resources [57]. EfficientNetB0 achieves a compromise between performance and efficiency through its advanced compound scaling strategy [58]. All three models have demonstrated strong performance in transfer learning scenarios, particularly when applied to mid-sized datasets as used in this research.

Each of the pretrained CNN architectures (DenseNet201, MobileNetV2, and EfficientNetB0) was modified to perform five-class classification by substituting the original top layers with a customized classification head. This newly designed head comprised additional convolutional and max-pooling layers, integrated with dropout for regularization, and concluded with a dense layer employing softmax activation. These architectural adjustments were consistently implemented across all models to maintain uniformity and enable a fair comparative analysis.

A total of 12 experiments were conducted by combining architectural modifications and hyperparameter tuning to evaluate performance and mitigate overfitting. The configuration of the modified DenseNet201 architecture used in the experiments is summarized in Table 2.

Table 2. DenseNet201 CNN Model Architecture with Pretained Model

Layer	Output Shape 1-2	Number of Output Shape 3-4		Number of
		Parameters		Parameters
DenseNet201	(None, 7, 7, 1920)	18321984	(None, 4, 4, 1920)	18321984
Conv2D	(None, 7, 7, 32)	552992	(None, 4, 4, 32)	552992
MaxPooling2D	(none3, 3, 32)	0	(None, 2, 2, 32)	0
Dropout	(none, 3, 3, 32)	0	(None, 2, 2, 32)	0
Flatten	(none, 288)	0	(None, 128)	0
Dense	(none, 5)	1445	(None, 5)	645

## 2.4. Training

After defining the model architectures with structural modifications, each CNN model (DenseNet201, MobileNetV2, and EfficientNetB0) was trained on both original and augmented datasets. The training phase aimed to optimize model performance across multiple configurations by adjusting image resolution, batch size, learning rate, and dropout rate.

The training procedure utilized the Adam optimization algorithm with two distinct learning rate configurations (0.0001 and 0.00001). Categorical cross-entropy was employed as the loss function, as it is suitable for multiclass classification tasks. To mitigate overfitting, dropout layers with rates of 0.2 and 0.5 were incorporated, alongside the application of early stopping based on validation loss monitoring. Each model was trained for 25 epochs using batch sizes of either 32 or 64.

Each model was trained on RGB images normalized to the [0,1] range and resized to either 224×224 or 128×128 pixels. An 80-10-10 split was applied to the dataset, allocating samples for training, validation, and testing, respectively.

Four experimental configurations were designed to evaluate the effect of data balancing and hyperparameter variation:

- Experiment 1: No data augmentation; image size: 224×224, batch size: 64, dropout : 0.2, learning rate: 0.0001.
- Experiment 2: Augmented dataset; image size: 224×224, batch size: 64, dropout: 0.2, learning rate: 0.0001.
- Experiment 3: Augmented dataset; image size: 128×128, batch size: 32, dropout: 0.2, learning rate: 0.0001.
- Experiment 4: Augmented dataset; image size: 128×128, batch size: 32, dropout: 0.5, learning rate: 0.00001.

Each CNN model was evaluated under all four experimental settings, resulting in a total of 12 experiments. Training progress was monitored using training and validation accuracy and loss curves, enabling observation of learning behavior and convergence patterns. The most optimal model from each configuration was selected based on the combination of highest validation accuracy and lowest validation loss, reflecting strong generalization performance.

#### 2.5. Testing

After training, each model was evaluated on the testing subset. Performance metrics included accuracy, precision, recall, and F1-score, calculated from the confusion matrix [59]. These metrics were used to identify the most effective model configuration for solar module surface defect classification.

## 3. Results and Discussion

The dataset used in this research consists of RGB images representing five types of surface conditions in solar modules: clean, dirt, burn, crack, and snail track Fig. 2. displays representative samples from each category used for model development. A sample dataset of solar panel images categorized into five classes: Burn, Clean, Crack, Dirt, and Snail Track. Each row displays representative examples of these conditions, showing the visual differences and defects that may occur in photovoltaic modules. The Burn category highlights panels with localized burn marks, while Clean panels appear undamaged and clear. The Crack category shows fractures across the cells, and Dirt panels are covered with dust or debris that obstructs sunlight. Finally, Snail Track panels exhibit dark discoloration lines resembling snail trails. This dataset provides a diverse collection of labeled images useful for training and evaluating machine learning models in solar panel defect detection.

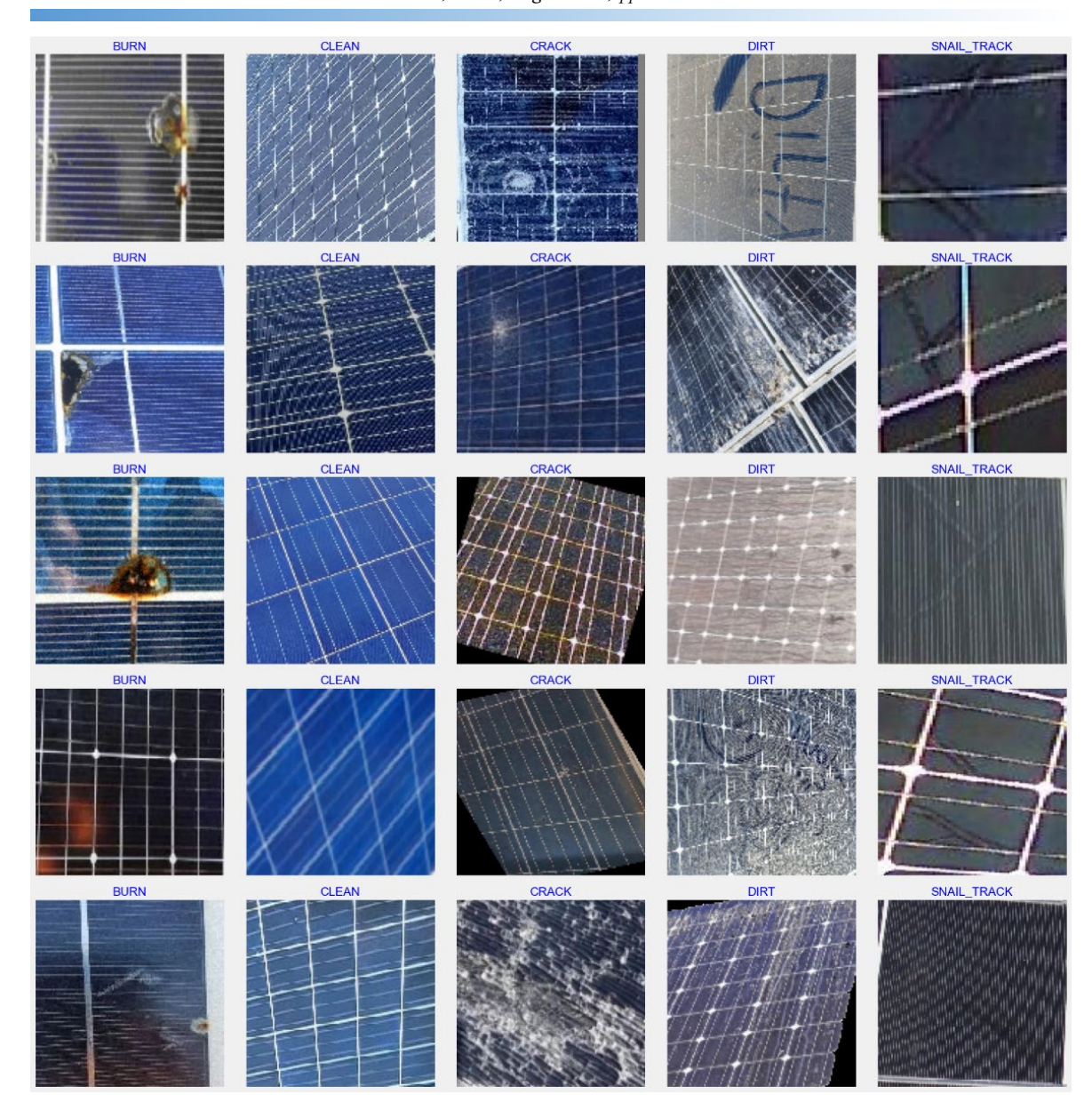


Fig. 2. Sample dataset consisting of five categories

## 3.1. Training Results

The accuracy and loss of training from DenseNet201, MobilenetV2, and EfficientNetB0 using epochs 25 is shown in Table 3. The accuracy and loss values obtained during training and validation for the pretrained models DenseNet201, MobileNetV2, and EfficientNetB0 across four experiments each. Overall, the results indicate strong training performance, with most experiments achieving near-perfect training accuracy (>98%), although the gap between training and validation values varies. DenseNet201 generally shows high accuracy and low loss, with Experiment 2 achieving the best validation accuracy (97.37%) and a small accuracy gap (2.57%). MobileNetV2 also performs well, though some experiments, such as 1 and 3, display a higher gap between training and validation (6–8%), suggesting potential overfitting. EfficientNetB0 achieves competitive results, with Experiment 2 showing the highest validation accuracy (95.94%) and a small gap, while Experiment 4 records a drop in both training and validation accuracy (85.53% and 87.60%, respectively). In summary, DenseNet201 demonstrates the most stable and consistently high validation performance, while EfficientNetB0 and MobileNetV2 deliver strong but slightly more variable results.

Table of Treatment and Essa value of Training							
Pre-trained Model	Experiments	Train Loss	Train Acc	Valid Loss	Valid Acc	GAP Loss	GAP Acc
DenseNet201	1	0.02	99.93%	0.21	92.24%	0.19	7.69%
DenseNet201	2	0.01	99.94%	0.08	97.37%	0.07	2.57%
DenseNet201	3	0.01	99.84%	0.14	95.91%	0.13	3.93%
DenseNet201	4	0.30	89.77%	0.29	90.53%	0.01	0.76%
MobilenetV2	1	0.01	99.83%	0,27	91.41%	0.26	8.42%
MobilenetV2	2	0.01	99.96%	0.18	93.79%	0.17	6.17%
MobilenetV2	3	0.01	99.81%	0.28	93.22%	0.28	6.59%
MobilenetV2	4	0.31	89.42%	0.35	88.19%	0.04	1.23%
EfficientNetB0	1	0.07	98.54%	0.29	91.41%	0.22	7.13%
EfficientNetB0	2	0.03	99.33%	0.09	95.94%	0.06	3.39%
EfficientNetB0	3	0.05	98.58%	0.15	95.56%	0.11	3.02%
EfficientNetB0	4	0.41	85.53%	0.36	87.60%	0.06	2.07%

Table 3. Accuracy and Loss Value of Training

Based on Table 3, the highest training accuracy (99.96%) was achieved by MobilenetV2 in experiment 2. However, its relatively large validation accuracy GAP (6.17%) indicates potential overfitting. In contrast, DensetNet201 in experiment 2 achieved a high validation accuracy of 97.37% with a smaller accuracy GAP (2.57%), demonstrating better generalization. The GAP metric, which represents the discrepancy between training and validation accuracy, is used to assess the model's ability to generalize to unseen data.

A lower GAP value indicates consistent performance across training and validation sets, suggesting minimal overfitting. In contrast, a higher GAP reflects potential overfitting, where the model has likely memorized the training data instead of learning generalizable patterns, thereby diminishing its effectiveness on new inputs. Among the three architectures, DenseNet201 showed the most consistent performance across different scenarios, balancing high accuracy with robust generalization. Furthermore, a comparison of the training result graphs of the three pre-training models with several trials is shown in Table 4.

The training results of three pre-trained models: DenseNet201, MobileNetV2, and EfficientNetB0, across four experimental runs each. For every experiment, the corresponding training and validation graphs are shown in terms of loss and accuracy. The loss graphs demonstrate a consistent downward trend across epochs, with varying convergence speeds depending on the model and experiment, while the accuracy graphs show the learning progression toward higher performance, generally stabilizing after several epochs. DenseNet201 and EfficientNetB0 exhibit smoother convergence with relatively balanced training and validation curves, whereas MobileNetV2 shows fluctuations in some experiments but still achieves strong accuracy. Overall, these results provide a visual comparison of each model's training behavior and performance stability across multiple runs.

Based on Table 4, the DenseNet201 models consistently demonstrates fast and stable convergence, with low validation loss and high, consistent validation accuracy, particularly in experiments 3 and 4. This indicates that the model effectively learns relevant features without significant overfitting. Meanwhile, MobileNetV2 shows a reasonable trend of increasing accuracy but with slight fluctuations in the loss values, especially in experiments 2 and 3, suggesting decent performance that is, however, not as optimal as DenseNet201. EfficientNetB0 exhibits balanced performance, with steadily decreasing loss curves and progressively improving validation accuracy across experiments, although it does not reach the same level of accuracy as DenseNet201. Overall, these results suggest that the DenseNet201 architecture outperforms the other two in handling the task of solar module surface defect classification.

Table 4. Graph of Training Results

Table 4. Graph of Training Results							
Pre-trained Model	Experiments	Graph Loss	Graph Accuracy				
DenseNet201	1	The strip and variable Lists  The st	Section 1975				
DenseNet201	2	Transmitted and statement and	Exercises and variation for more deep to the second of the				
DenseNet201	3	Transfer or of Valuation Labor Section 1.	Travering and Yan Madaran Alayseary  100  100  100  100  100  100  100  1				
DenseNet201	4	The country and the country an	Tracety and falled an Anamay  Tracet				
MobilenetV2	1	Transmitted and Vandade Look  The American American  The American Am	Training and Statement regions are				
MobilenetV2	2	Transport Videntico Indo	Tracerong and Vandadors Assuming				
MobilenetV2	3	Training and Variations came  Traini	Trotaing and Valladam Astoniansy  Totaling and Valladam Astoniansy  Totali				
MobilenetV2	4	Trowney and visit deposit Long.	Comment and Voluntiation Associatory  Transmission and Voluntiation				
EfficientNetB0	1	Transing and Veledate Load   Average   Average	Total Space Visitation Assessed				
EfficientNetB0	2	Transfer and Valdedory, Lond  Transf	The state of the s				
EfficientNetB0	3	Taming and Valentini List  Valency  Val	Training and Variation Accoracy  To the region of Variation Accoracy  The state of Variation Accora				
EfficientNetB0	4	Total ring and Validation (Lenia Total plans and Total plans a	Tableman and Orderdon Accountry of the Control of t				

# 3.2. Testing Results

To evaluate generalization, all trained models were tested using the testing subset. The testing results is shown in Table 5, consisting of accuracy, precision, recall and F1 score values.

Pre-trained Model	Experiments	Accuracy	Precision	Recall	F1 Score
DenseNet201	1	94.17	94.17	94.17	94.17
DenseNet201	2	97.85	97.82	97.79	97.81
DenseNet201	3	93.44	93.44	93.44	93.44
DenseNet201	4	89.58	90.53	89.58	90.05
MobilenetV2	1	92.78	92.78	92.78	92.78
MobilenetV2	2	94.98	94.98	94.98	94.98
MobilenetV2	3	88.76	88.76	88.76	88.76
MobilenetV2	4	85.71	86.73	85.71	86.22
EfficientNetB0	1	91.94	91.94	91.94	91.94
EfficientNetB0	2	97.25	97.25	97.25	97.25
EfficientNetB0	3	94.61	94.61	94.61	94.61
EfficientNetB0	4	87.47	87.57	87.47	87.52

Table 5. Testing Results Using Transfer Learning of 3 Pre-trained CNN Models

According to Table 5, the test results of the three models using datasets with augmentation to balance the number of datasets have higher accuracy, precision, recall, and F1-score values compared to datasets without augmentation. The percentage increase in evaluation results is 2% to 5%. Other experiments by changing hyperparameters produce evaluation results of 2% to 10%. Despite similar accuracy, DenseNet201 provided more stable precision and recall, likely due to its dense connectivity that improves feature reuse and learning depth. MobileNetV2 delivers strong performance with minimal complexity, making it suitable for use in resource-constrained environments, despite its lower accuracy compared to the other two model presets.

In terms of model efficiency, MobileNetV2 offers the smallest model size and fastest inference time, making it attractive for edge deployment despite its slightly lower classification accuracy. DenseNet201, although achieving the highest accuracy (97.85%), has a relatively larger parameter count and longer inference time. EfficientNetB0 provides a balance between performance and computational cost. These trade-offs should be considered based on the computational resources available in practical deployment

Table 6 highlights a clear performance gap across models. Deep learning approaches, particularly DenseNet201 and EfficientNetB0, achieved the highest metrics across all categories, with most scores around or above 97%. These results significantly outperform traditional machine learning methods such as SVM (73.60%) and Random Forest (81.51%), underscoring the latter's limitations in modeling complex visual patterns and texture-based defects. While the shallow CNN demonstrated reasonable performance (84.53%), it lagged behind deeper transfer learning models. This gap affirms the effectiveness of leveraging pre-trained architectures that are capable of capturing rich hierarchical features essential for distinguishing subtle morphological differences in solar module surface defects. Overall, the results validate the superiority of deep learning, particularly transfer learning, in handling highdimensional image data for surface defect classification tasks.

Model Accuracy Precision Recall F1 Score SVM 73.60 74.43 73.60 73.22 Random Forest 81.51 81.46 81.51 81.39 Shallow CNN 84.53 85.33 84.53 84.34 DenseNet201 97.85 97.82 97.79 97.81 MobilenetV2 94.98 94.98 94.98 94.98 EfficientNetB0 97.25 97.25 97.25 97.25

Table 6. Performance Comparison Across Models

Fig. 3 presents the confusion matrix illustrating the classification performance of the best-performing model. The diagonal elements indicate correct predictions for each defect category, with burn, clean, and dirt showing particularly strong results, achieving 167, 169, and 187 true positives, respectively. Crack and snail track classes also demonstrate solid performance with 139 and 157 correct classifications, though minor misclassifications occurred across several categories.

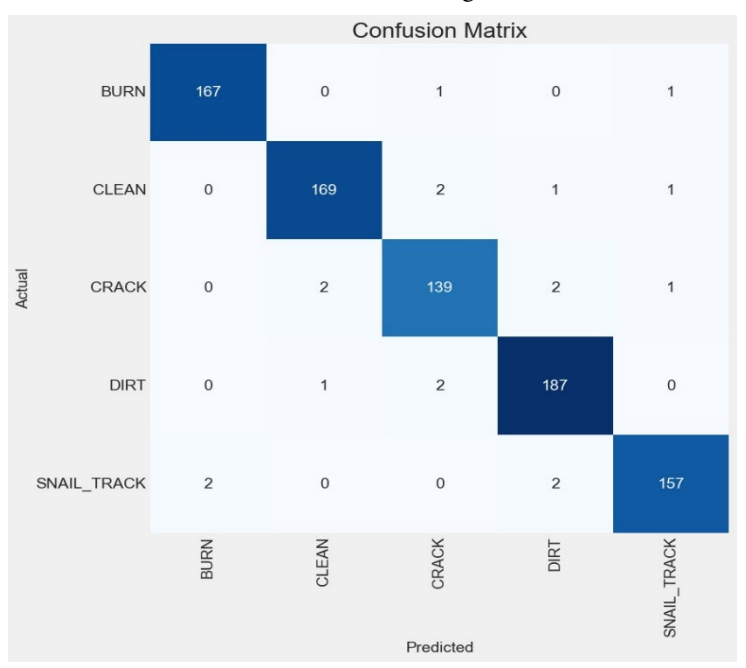
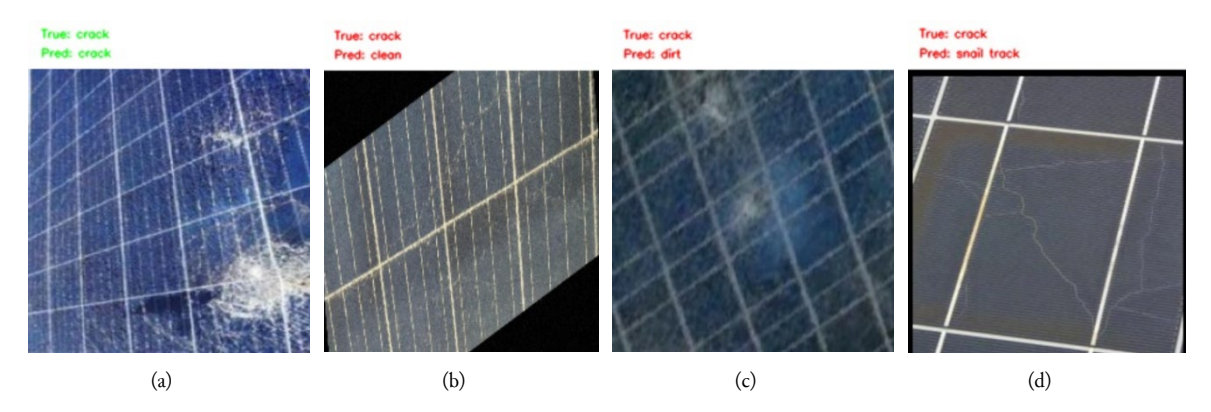


Fig. 3. Confusion matrix the highest accuracy in testing

The model achieved strong overall performance but struggled with consistent misclassification of the crack class. As illustrated in Fig. 4, although some cracks were correctly identified (a), others were mislabeled as clean (b), dirt (c), or snail track (d). These errors likely stem from various factors: the crack in (b) appears subtle and low-contrast, making it easily mistaken for a clean surface; the image in (c) shows a crack pattern that blends with textural noise, resembling dirt; while (d) presents visual traits similar to snail tracks, such as diffuse patterns and irregular edges. These cases highlight the model's difficulty in distinguishing fine-grained structural anomalies, particularly under variable lighting and surface noise conditions. Although lighting metadata was not available for explicit evaluation, the results suggest the need for more robust feature extraction techniques, such as edge enhancement, texture descriptors, or multi-scale representations, to improve crack detection under real-world conditions.



**Fig. 4.** Examples of misclassified images: (a) correctly classified crack, (b) crack mislabeled as clean, (c) crack mislabeled as dirt, (d) crack mislabeled as snail track

While traditional thermal imaging and EL methods are widely used for defect detection, they often require specialized equipment and are sensitive to environmental conditions. In contrast, the RGB-based

classification approach proposed in this research offers a cost-effective and scalable alternative, particularly suitable for early-stage detection using standard imaging devices in field environments.

Despite achieving high classification performance, this study has not evaluated computational efficiency metrics such as training time, inference speed, and model size. These aspects are crucial for real-world deployment, particularly in edge-based or embedded systems for solar module monitoring. Future research will include a thorough assessment of these efficiency parameters to determine the feasibility of implementing the proposed models in practical environments.

The CNN-based classification model developed in this research can be effectively integrated into existing solar power plant monitoring systems to improve inspection accuracy and maintenance efficiency. By utilizing drone or fixed camera systems already deployed in many solar farms, images of solar module surfaces can be captured routinely and analyzed automatically using the trained model. Integration with edge computing devices, such as NVIDIA Jetson or Raspberry Pi, enables on-site image processing, reducing latency and the need for high-bandwidth data transmission. This real-time detection allows maintenance teams to quickly identify and respond to surface defects such as cracks, burns, or dirt accumulation.

Furthermore, the model's output can be linked to Supervisory Control and Data Acquisition (SCADA) systems or IoT dashboards, allowing operators to monitor module conditions visually and receive automated alerts for detected anomalies. Maintenance requests can be generated and prioritized based on defect type and severity through integration with Computerized Maintenance Management Systems (CMMS). Over time, the system can support predictive maintenance by tracking recurring defect patterns. This practical integration offers a scalable and cost-effective solution for improving the reliability, responsiveness, and operational efficiency of solar power plants.

#### 4. Conclusion

This research developed a classification model for solar module surface defects using Deep Convolutional Neural Networks (CNNs) with transfer learning. The model categorized five visually observable defect types : clean, dirt, burn, crack, and snail track, using a combination of field-acquired and public RGB datasets. To address data imbalance, augmentation techniques were applied. Among the three evaluated models: DenseNet201, MobileNetV2, and EfficientNetB0. DenseNet201 achieved the highest accuracy of 97.01% with a 224×224 image size, batch size of 64, dropout rate of 0.2, and learning rate of 0.0001. The findings highlight the capability of CNN-based image classification to enhance solar module inspection processes. The proposed model can be integrated into solar plant monitoring systems to support faster, more accurate identification of surface anomalies, thereby enhancing preventive maintenance and operational reliability. Research efforts moving forward will be directed toward advancing the deployment of the proposed system in practical settings. A key limitation of the current research is the reliance on RGB imagery without direct comparison to thermal imaging for real-time fault detection, this will be explored in future work. To improve detection accuracy, automated hyperparameter optimization will be implemented, reducing manual tuning efforts. Dataset limitations will be addressed through GAN-based augmentation, simulating diverse lighting conditions and rare defect patterns. For real-world deployment, model efficiency will be optimized for edge devices (e.g., NVIDIA Jetson), coupled with user-friendly diagnostic interfaces. Additionally, future work will include a comprehensive evaluation of computational efficiency metrics (such as training time, inference speed, and model size) to ensure the model's feasibility for real-time deployment in embedded solar monitoring systems. These steps aim to bridge the gap between laboratory validation and field implementation in solar power plants.

## Acknowledgment

Thanks are given to the Directorate of Research, Technology, and Community Service Ministry of Education, Culture, Research, and Technology, Indonesia (Grant No. 105/E5/PG.02.00.PL/2024), for funding for the author's research, Gunadarma University and the PLN Institute of Technology for supporting research activities.

#### **Declarations**

**Author contribution.** All authors contributed equally to the main contributor to this paper. All authors read and approved the final paper.

**Funding statement.** This research was funded by the Directorate of Research, Technology, and Community Service Ministry of Education, Culture, Research, and Technology, Indonesia, under Grant No. 105/E5/PG.02.00.PL/2024.

**Conflict of interest.** The authors declare no conflict of interest.

**Additional information.** No additional information is available for this paper.

## References

- [1] U. Kumar, S. Mishra, and K. Dash, "An IoT and Semi-Supervised Learning-Based Sensorless Technique for Panel Level Solar Photovoltaic Array Fault Diagnosis," *IEEE Trans. Instrum. Meas.*, vol. 72, pp. 1–12, 2023, doi: 10.1109/TIM.2023.3287247.
- [2] K. Z. Mostofa and M. A. Islam, "Creation of an Internet of Things (IoT) system for the live and remote monitoring of solar photovoltaic facilities," *Energy Reports*, vol. 9, pp. 422–427, Oct. 2023, doi: 10.1016/j.egyr.2023.09.060.
- [3] N. El Yanboiy *et al.*, "Mejora de la detección de defectos superficiales en paneles solares con modelos VGG basados en IA," *Data Metadata*, vol. 2, p. 81, Dec. 2023, doi: 10.56294/dm202381.
- [4] R. B. Patil, A. Khalkar, S. Al-Dahidi, R. S. Pimpalkar, S. Bhandari, and M. Pecht, "A Reliability and Risk Assessment of Solar Photovoltaic Panels Using a Failure Mode and Effects Analysis Approach: A Case Study," *Sustainability*, vol. 16, no. 10, p. 4183, May 2024, doi: 10.3390/su16104183.
- [5] L. Alhmoud, "Why Does the PV Solar Power Plant Operate Ineffectively?," *Energies*, vol. 16, no. 10, p. 4074, May 2023, doi: 10.3390/en16104074.
- [6] M. L. Katche, A. B. Makokha, S. O. Zachary, and M. S. Adaramola, "A Comprehensive Review of Maximum Power Point Tracking (MPPT) Techniques Used in Solar PV Systems," *Energies*, vol. 16, no. 5, p. 2206, Feb. 2023, doi: 10.3390/en16052206.
- [7] S. Mamykin, R. Z. Shneck, B. Dzundza, F. Gao, and Z. Dashevsky, "A Novel Solar System of Electricity and Heat," *Energies*, vol. 16, no. 7, p. 3036, Mar. 2023, doi: 10.3390/en16073036.
- [8] K. Barbusiński *et al.*, "Influence of Environmental Conditions on the Electrical Parameters of Side Connectors in Glass–Glass Photovoltaic Modules," *Energies*, vol. 17, no. 3, p. 680, Jan. 2024, doi: 10.3390/en17030680.
- [9] A. K. Schnatmann *et al.*, "Investigating the Technical Reuse Potential of Crystalline Photovoltaic Modules with Regard to a Recycling Alternative," *Sustainability*, vol. 16, no. 3, p. 958, Jan. 2024, doi: 10.3390/su16030958.
- [10] I. Gunes, "Comparison of PV Panels and Non-Planar PV Surfaces in Terms of Pollution," in 2025 IEEE Texas Power and Energy Conference (TPEC), Feb. 2025, pp. 1–5, doi: 10.1109/TPEC63981.2025.10906853.
- [11] S. Hassan and M. Dhimish, "A Survey of CNN-Based Approaches for Crack Detection in Solar PV Modules: Current Trends and Future Directions," *Solar*, vol. 3, no. 4, pp. 663–683, Dec. 2023, doi: 10.3390/solar3040036.
- [12] H. Al Mahdi, P. G. Leahy, M. Alghoul, and A. P. Morrison, "A Review of Photovoltaic Module Failure and Degradation Mechanisms: Causes and Detection Techniques," *Solar*, vol. 4, no. 1, pp. 43–82, Jan. 2024, doi: 10.3390/solar4010003.
- [13] J. Yang, M. Xin, and Q. Feng, "Automatic hot spot edge-detection method for photovoltaic aerial infrared image," in *Third International Conference on Artificial Intelligence, Virtual Reality, and Visualization (AIVRV 2023)*, Nov. 2023, vol. 12923, p. 24, doi: 10.1117/12.3011341.
- [14] M. U. Ali, H. F. Khan, M. Masud, K. D. Kallu, and A. Zafar, "A machine learning framework to identify the hotspot in photovoltaic module using infrared thermography," *Sol. Energy*, vol. 208, pp. 643–651, Sep. 2020, doi: 10.1016/j.solener.2020.08.027.

- [15] A. Singh Chaudhary and D. K. Chaturvedi, "Analyzing Defects of Solar Panels under Natural Atmospheric Conditions with Thermal Image Processing," *Int. J. Image, Graph. Signal Process.*, vol. 10, no. 6, pp. 10–21, Jun. 2018, doi: 10.5815/ijigsp.2018.06.02.
- [16] S. Djordjevic, D. Parlevliet, and P. Jennings, "Detectable faults on recently installed solar modules in Western Australia," *Renew. Energy*, vol. 67, pp. 215–221, Jul. 2014, doi: 10.1016/j.renene.2013.11.036.
- [17] M. Dhimish and V. Holmes, "Solar cells micro crack detection technique using state-of-the-art electroluminescence imaging," *J. Sci. Adv. Mater. Devices*, vol. 4, no. 4, pp. 499–508, Dec. 2019, doi: 10.1016/j.jsamd.2019.10.004.
- [18] J. P. C. Barnabé, L. P. Jiménez, G. Fraidenraich, E. R. De Lima, and H. F. Dos Santos, "Quantification of Damages and Classification of Flaws in Mono-Crystalline Photovoltaic Cells Through the Application of Vision Transformers," *IEEE Access*, vol. 11, pp. 112334–112347, 2023, doi: 10.1109/ACCESS.2023.3322653.
- [19] M. S. H. Onim *et al.*, "SolNet: A Convolutional Neural Network for Detecting Dust on Solar Panels," *Energies*, vol. 16, no. 1, p. 155, Dec. 2022, doi: 10.3390/en16010155.
- [20] I. Bodnár, D. Matusz-Kalász, and R. R. Boros, "Exploration of Solar Panel Damage and Service Life Reduction Using Condition Assessment, Dust Accumulation, and Material Testing," *Sustainability*, vol. 15, no. 12, p. 9615, Jun. 2023, doi: 10.3390/su15129615.
- [21] A. Ghahremani, S. D. Adams, M. Norton, S. Y. Khoo, and A. Z. Kouzani, "Delamination Techniques of Waste Solar Panels: A Review," *Clean Technol.*, vol. 6, no. 1, pp. 280–298, Feb. 2024, doi: 10.3390/cleantechnol6010014.
- [22] U. Hijjawi, S. Lakshminarayana, T. Xu, G. Piero Malfense Fierro, and M. Rahman, "A review of automated solar photovoltaic defect detection systems: Approaches, challenges, and future orientations," *Sol. Energy*, vol. 266, p. 112186, Dec. 2023, doi: 10.1016/j.solener.2023.112186.
- [23] S. A. Memon, Q. Javed, W.-G. Kim, Z. Mahmood, U. Khan, and M. Shahzad, "A Machine-Learning-Based Robust Classification Method for PV Panel Faults," *Sensors*, vol. 22, no. 21, p. 8515, Nov. 2022, doi: 10.3390/s22218515.
- [24] H. Munawer Al-Otum, "Deep learning-based automated defect classification in Electroluminescence images of solar panels," *Adv. Eng. Informatics*, vol. 58, p. 102147, Oct. 2023, doi: 10.1016/j.aei.2023.102147.
- [25] N. A. M. Roslan, N. M. Diah, Z. Ibrahim, Y. Munarko, and A. E. Minarno, "Automatic plant recognition using convolutional neural network on Malaysian medicinal herbs: the value of data augmentation," *Int. J. Adv. Intell. Informatics*, vol. 9, no. 1, pp. 136–147, 2023, doi: 10.26555/ijain.v9i1.1076.
- [26] H. Haviluddin and R. Alfred, "Multi-step CNN forecasting for COVID-19 multivariate time-series," *Int. J. Adv. Intell. Informatics*, vol. 9, no. 2, p. 176, Jul. 2023, doi: 10.26555/ijain.v9i2.1080.
- [27] X. Zhao, L. Wang, Y. Zhang, X. Han, M. Deveci, and M. Parmar, "A review of convolutional neural networks in computer vision," *Artif. Intell. Rev.*, vol. 57, no. 4, p. 99, Mar. 2024, doi: 10.1007/s10462-024-10721-6.
- [28] A. Serikbay, M. Bagheri, A. Zollanvari, and B. T. Phung, "Ensemble Pretrained Convolutional Neural Networks for the Classification of Insulator Surface Conditions," *Energies*, vol. 17, no. 22, p. 5595, Nov. 2024, doi: 10.3390/en17225595.
- [29] A. Younesi, M. Ansari, M. Fazli, A. Ejlali, M. Shafique, and J. Henkel, "A Comprehensive Survey of Convolutions in Deep Learning: Applications, Challenges, and Future Trends," *IEEE Access*, vol. 12, pp. 41180–41218, 2024, doi: 10.1109/ACCESS.2024.3376441.
- [30] S. Y. Prasetyo, G. Z. Nabiilah, Z. N. Izdihar, and S. M. Isa, "Pneumonia Detection on X-Ray Imaging using Softmax Output in Multilevel Meta Ensemble Algorithm of Deep Convolutional Neural Network Transfer Learning Models," *Int. J. Adv. Intell. Informatics*, vol. 9, no. 2, p. 319, Jul. 2023, doi: 10.26555/ijain.v9i2.884.
- [31] S. Hassan and M. Dhimish, "Dual spin max pooling convolutional neural network for solar cell crack detection," *Sci. Rep.*, vol. 13, no. 1, p. 11099, Jul. 2023, doi: 10.1038/s41598-023-38177-8.
- [32] A. Shihavuddin *et al.*, "Image based surface damage detection of renewable energy installations using a unified deep learning approach," *Energy Reports*, vol. 7, pp. 4566–4576, Nov. 2021, doi: 10.1016/j.egyr.2021.07.045.

- [33] Z. Zha, D. Shi, X. Chen, H. Shi, and J. Wu, "Classification of Appearance Quality of Red Grape Based on Transfer Learning of Convolution Neural Network," *Agronomy*, vol. 13, no. 8, p. 2015, Jul. 2023, doi: 10.3390/agronomy13082015.
- [34] M. Hasanat, W. Khan, N. Minallah, N. Aziz, and A.-U.-R. Durrani, "Performance evaluation of transfer learning based deep convolutional neural network with limited fused spectro-temporal data for land cover classification," *Int. J. Electr. Comput. Eng.*, vol. 13, no. 6, p. 6882, Dec. 2023, doi: 10.11591/ijece.v13i6.pp6882-6890.
- [35] X. Song and Y. Liu, "Defect Detection of Solar Panel Based on DenseNet Network," in *Advances in Transdisciplinary Engineering*, vol. 35, IOS Press, 2023, pp. 661–669, doi: 10.3233/ATDE230093.
- [36] S. Matarneh, F. Elghaish, F. Pour Rahimian, E. Abdellatef, and S. Abrishami, "Evaluation and optimisation of pre-trained CNN models for asphalt pavement crack detection and classification," *Autom. Constr.*, vol. 160, p. 105297, Apr. 2024, doi: 10.1016/j.autcon.2024.105297.
- [37] M. A. El-Rashidy, "An efficient and portable solar cell defect detection system," *Neural Comput. Appl.*, vol. 34, no. 21, pp. 18497–18509, Nov. 2022, doi: 10.1007/s00521-022-07464-2.
- [38] Y. Zou, L. Wu, C. Zuo, L. Chen, B. Zhou, and H. Zhang, "White blood cell classification network using MobileNetv2 with multiscale feature extraction module and attention mechanism," *Biomed. Signal Process. Control*, vol. 99, p. 106820, Jan. 2025, doi: 10.1016/j.bspc.2024.106820.
- [39] Z. Zhao, E. B. A. Bakar, N. B. A. Razak, and M. N. Akhtar, "Corrosion image classification method based on EfficientNetV2," *Heliyon*, vol. 10, no. 17, p. e36754, Sep. 2024, doi: 10.1016/j.heliyon.2024.e36754.
- [40] Z. B. Duranay, "Fault Detection in Solar Energy Systems: A Deep Learning Approach," *Electronics*, vol. 12, no. 21, p. 4397, Oct. 2023, doi: 10.3390/electronics12214397.
- [41] M. Gao, Y. Xie, P. Song, J. Qian, X. Sun, and J. Liu, "A Definition Rule for Defect Classification and Grading of Solar Cells Photoluminescence Feature Images and Estimation of CNN-Based Automatic Defect Detection Method," *Crystals*, vol. 13, no. 5, p. 819, May 2023, doi: 10.3390/cryst13050819.
- [42] M. W. Akram *et al.*, "CNN based automatic detection of photovoltaic cell defects in electroluminescence images," *Energy*, vol. 189, p. 116319, Dec. 2019, doi: 10.1016/j.energy.2019.116319.
- [43] M. R. Rahman, S. Tabassum, E. Haque, M. M. Nishat, F. Faisal, and E. Hossain, "CNN-based Deep Learning Approach for Micro-crack Detection of Solar Panels," in *2021 3rd International Conference on Sustainable Technologies for Industry 4.0 (STI)*, Dec. 2021, pp. 1–6, doi: 10.1109/STI53101.2021.9732592.
- [44] C. Bu, T. Liu, T. Wang, H. Zhang, and S. Sfarra, "A CNN-Architecture-Based Photovoltaic Cell Fault Classification Method Using Thermographic Images," *Energies*, vol. 16, no. 9, p. 3749, Apr. 2023, doi: 10.3390/en16093749.
- [45] H. Chen, Y. Pang, Q. Hu, and K. Liu, "Solar cell surface defect inspection based on multispectral convolutional neural network," *J. Intell. Manuf.*, vol. 31, no. 2, pp. 453–468, Feb. 2020, doi: 10.1007/s10845-018-1458-z.
- [46] T. Rahman *et al.*, "Investigation of Degradation of Solar Photovoltaics: A Review of Aging Factors, Impacts, and Future Directions toward Sustainable Energy Management," *Energies*, vol. 16, no. 9, p. 3706, Apr. 2023, doi: 10.3390/en16093706.
- [47] A. S. Al-Waisy *et al.*, "Identifying defective solar cells in electroluminescence images using deep feature representations," *PeerJ Computer Science*, vol. 8. PeerJ Inc., p. e992, May 19, 2022, doi: 10.7717/peerjcs.992/table-9.
- [48] Afroz, "Solar Panel Images Clean and Faulty Images," *Kaggle*, 2023. [Online]. Available at: https://www.kaggle.com/datasets/pythonafroz/solar-panel-images.
- [49] "solar panels fault," *Roboflow Universe Search*, 2025. [Online]. Available at: https://universe.roboflow.com/search?q=solar+panels+fault.
- [50] A. Pendota and S. S. Channappayya, "Are Deep Learning Models Pre-trained on RGB Data Good Enough for RGB-Thermal Image Retrieval?," in 2024 IEEE/CVF Conference on Computer Vision and Pattern Recognition Workshops (CVPRW), Jun. 2024, pp. 4287–4296, doi: 10.1109/CVPRW63382.2024.00432.

- [51] P. Purnawansyah, A. Adnan, H. Darwis, A. P. Wibawa, T. Widyaningtyas, and H. Haviluddin, "Ensemble semi-supervised learning in facial expression recognition," *Int. J. Adv. Intell. Informatics*, vol. 11, no. 1, p. 1, Feb. 2025, doi: 10.26555/ijain.v11i1.1880.
- [52] D. Sathya, S. B. Jeniffer, R. S. J, L. M, and R. R. G, "Efficient Traffic Sign Detection Using CNNs: A Scalable Deep Learning Model," in 2024 Eighth International Conference on Parallel, Distributed and Grid Computing (PDGC), Dec. 2024, pp. 693–699, doi: 10.1109/PDGC64653.2024.10984039.
- [53] E. Jain and A. Singh, "Efficient Handwritten Digit Classification using Convolutional Neural Networks: A Robust Approach with Data Augmentation," in 2024 3rd International Conference on Automation, Computing and Renewable Systems (ICACRS), Dec. 2024, pp. 1234–1239, doi: 10.1109/ICACRS62842.2024.10841545.
- [54] L. Menglin, X. Qiang, Z. Peng, Z. Dahua, H. Lizhi, and H. Baiji, "Encrypted Traffic Identification in Power IoT based on CNN with Batch Normalization," in 2024 6th International Conference on Electrical Engineering and Control Technologies (CEECT), Dec. 2024, pp. 136–142, doi: 10.1109/CEECT63656.2024.10898407.
- [55] E. Pintelas, I. E. Livieris, S. Kotsiantis, and P. Pintelas, "A multi-view-CNN framework for deep representation learning in image classification," *Comput. Vis. Image Underst.*, vol. 232, p. 103687, Jul. 2023, doi: 10.1016/j.cviu.2023.103687.
- [56] J. Jerome Vasanth, S. Naveen Venkatesh, V. Sugumaran, and V. S. Mahamuni, "Enhancing Photovoltaic Module Fault Diagnosis with Unmanned Aerial Vehicles and Deep Learning-Based Image Analysis," *Int. J. Photoenergy*, vol. 2023, no. 1, pp. 1–17, Jul. 2023, doi: 10.1155/2023/8665729.
- [57] J. Lee, J. Park, and Y. Lee, "Toward Efficient Cancer Detection on Mobile Devices," *IEEE Access*, vol. 13, pp. 34613–34626, 2025, doi: 10.1109/ACCESS.2025.3543838.
- [58] M. R. M. Kamal, S. Shahbudin, and F. Y. A. Rahman, "Photovoltaic (PV) Module Defect Image Classification Analysis Using EfficientNetV2 Architectures," in 2023 IEEE 14th Control and System Graduate Research Colloquium (ICSGRC), Aug. 2023, pp. 236–241, doi: 10.1109/ICSGRC57744.2023.10215491.
- [59] I. Markoulidakis, I. Rallis, I. Georgoulas, G. Kopsiaftis, A. Doulamis, and N. Doulamis, "Multiclass Confusion Matrix Reduction Method and Its Application on Net Promoter Score Classification Problem," *Technologies*, vol. 9, no. 4, p. 81, Nov. 2021, doi: 10.3390/technologies9040081.